Title

Application of Electrical Resistivity, Seismic Refraction, And Multi-Channel Analysis of Surface Waves Method to Investigate a site proposed for construction at University of Ghana, In Accra Ghana.

*Emmanuel. Aduse-Poku, Thomas Kaku Armah, Paulina Ekua Amponsah

*University of Ghana

Department of Earth Science,

P.O.Box LG 50

Accra – Ghana

*Corresponding Author

Phone : +233243282531

Email: adusepokuemmanuel2@gmail.com

Abstract

To deploy cost-effective techniques for subsurface assessments, Electrical Resistivity Tomography (ERT), Seismic Refraction Tomography (SRT), and Multichannel Analysis of Surface Waves (MASW) were applied to investigate a site proposed for the construction of a multi-story residential facility for Commonwealth Hall of the University of Ghana. The task was to identify buried metallic pipes, subsurface layers, bedrock depth, and classify the site soil. By using ERT, a map of possible locations of utility pipes has been developed to help assist their detection. Of the 71 locations identified as potential anomalous points, 6 are in areas with high instrument sensitivity, 46 are in areas of moderate instrument sensitivity and 19 are in areas of low instrument sensitivity. Geoelectric sections developed from four depth slices to show resistivity distribution at depth indicate that there are three distinct resistivity zones: resistivity zones less than 300 Ohm.m, between 300 Ohm.m and 2000 Ohm.m, and those greater than 2000 Ohm.m. Three velocity layers were inferred from SRT and the first layer is less than 1.400 km/s at an average depth of 4m. The second layer has a velocity between 1.400 km/s and 2.000 km/s at an average depth of about 7m and the third layer is at a depth greater than 10 m and has a velocity between 2.300 km/s and 3.600 km/s. The borehole report from SRT Line 400 suggests that the subsurface is made of laterites and a weathered quartzite formation. Moreover, the Vs30 parameter for this site has been estimated to be between 0.720 km/s and 0.760 km/s classifying the site as class C, suggesting weathered subsurface materials as well.

1.0 Background and Introduction

The Commonwealth Hall Alumni Association of the University of Ghana sought to embark on the construction of halls of residence, and before the site for construction would be deemed safe and competent to hold the facility, the subsurface geology was to be understood to avoid engineering problems (Martínez & Mendoza, 2011). Like all structurally engineered projects, there was the need to investigate the subsurface to determine the suitability of the subsurface material (Alabi et al., 2018) to support the structure. The geological processes of the site were to be well understood because knowledge of geology and geological processes effective within an area can have significant implications on locating the infrastructure and ensuring its safety and cost-effectiveness (Tyler et al., 2017). Due to the efficiency and cost-effective nature of geophysical methods compared to conventional site investigation techniques, environmental and engineering applications of surface geophysical techniques have gained wide interest (Reynold,2011) and this project applied three geophysical techniques to investigate the site.

electrical survey aims to determine the subsurface resistivity distribution by making measurements on the subsurface and from which the true resistivity of the subsurface can be estimated (Loke, 1999). The work of Vickery and Hobbs (2002) indicates that subsurface conducting pipes can either be a target or noise in geophysical surveying because they create strong signatures that can be detected. A subsurface conducting pipe will cause a reduction of resistivity from the background by 60%. (Vickery & Hobbs, 2002) and for a dipole-dipole array, the resistivity is reduced when the pipe is between the dipoles and gradually increases away from the dipoles underscoring the possibility of electrical resistivity being used in subsurface utility engineering.

Seismic refraction tomography (SRT) can be used in investigating shallow levels of the subsurface.2-Dimensional profiles can be developed from SRT including depth and distance which simplifies the characterization of relatively large volumes of the subsurface (Azwin et al., 2013). There has been an explosion in the use of SRT because it is a powerful tool to visualize subsurface layers. It has been used to delineate layers, bedrock topography, basement depth, the thickness of the weathered basement, and to characterize subsurface wave velocities (Azwin et al. 2013; Avalos et al. 2016; Kassie, 2019). (Araffa et al. (2014) have described Multi-Channel Analysis of Surface Wave (MASW) as the ‘‘work-horse’’ of engineering geophysics and has been widely applied to regolith mapping in geotechnical engineering as a fast noninvasive method employed to determine

near-surface shear wave velocity (Olafsdottir et al., 2018; Taipodia et al., 2020). It has been demonstrated that geophysics can provide solutions for determining subsurface properties and that different prospecting techniques are needed to build a realistic model of the subsurface structure (Araffa et al. 2014; Malehmir et al. 2013; Soupios et al. 2007). Therefore, three geophysical methods were applied for this investigation; Electrical resistivity method (ERT), Seismic Refraction Tomography (SRT) and, Multichannel Analysis of Surface Waves (MASW) method. ERT, SRT, and MASW were used to map metallic pipes, delineate velocity layers and define the shear wave velocity at 30m (VS30) respectively. Accordingly, the ERT results have been used to develop a geoelectric section to show areas of electrical resistivity as a function of resistivity meter sensitivity. The velocity layers of the subsurface have been delineated and the soil of the site has also been classified based on the National Earthquake Hazards Reduction Program (NERHP,2003)classification.

1.1 Literature Review

1.1.1 Site Investigation

Site investigation is the process by which geological, geotechnical, and other relevant information which might affect the construction or performance of a civil engineering or building project is acquired (Clayton et al., 1982).To avoid future engineering flaws, the geological processes of the chosen site must be well understood (Tyler et al., 2017) before a structure is installed. Geophysical techniques are gaining interest in site investigation and as emphasized by Soupios et al. (2007), the last decade has seen promising growth in the use of the technique for site investigation because the technique can be used for a different set of problems. For example, seismic refraction surveys can be used to estimate the depth to bedrock (Martínez & Mendoza, 2011), and electrical resistivity surveys can be used to identify the geoelectric nature of the subsurface which is relatable to voids or moisture contents of the soil according to Keary et al, (2002) and Ground Penetrating Radar (GPR) is also useful in locating buried utilities, bedrock depth, soil stratigraphy, water table depth, delineate and identify karst features (Davis et. Al., 1989).

In site investigation, geoelectrical and shallow seismic refraction methods are considered very important and are usually used in diverse ways, including groundwater exploration, foundation studies, and siting studies (Shebl et al., 2019). Consequently, the two geophysical methods are used in an enjoined way to better aid in interpretation and evaluate the significance and reliability of each result obtained (Leucci et al., 2007). Moreover, electrical resistivity tomography (ERT) and shallow seismic methods (SRT and MASW) are techniques for delineating the subsurface configurations like stratigraphy, structural elements, caves, and water-saturated zones (Araffa et al., 2014). Multi-channel surface wave analysis (MASW), and microtremor refraction techniques are also non-destructive seismic methods that can be used to assess shear wave velocity as a function of depth (Martin & Diehl, 2004).

1.1.2 Electrical Resistivity Tomography

The purpose of electrical survey is to determine the subsurface resistivity distribution, by making measurements on the subsurface and from which the true resistivity of the subsurface can be estimated (Loke, 1999). Measurements are processed and interpreted to relate to subsurface bodies like rocks, ore bodies, water resources, and buried utilities. The method has been used for a wide range of applications ranging from archaeological, hydrological, geotechnical, environmental, and mineral exploration problems (Auken et al., 2006; Loke et al., 2013). This wide usage of the electrical resistivity method is partly due to its versatility in many fields, including water exploration, environmental investigation, and mineral exploration engineering. For example, Nordiana et al. (2018) used 2D electrical tomography to assess the ground failure of an urban area in Selangor, Malaysia. Muchingami et al. (2012) combined 2D electrical resistivity tomography and 1D VES to produce a subsurface resistivity model to assess the availability of groundwater in the basaltic-greenstone formation of the Matsheumhlope well field in Bulawayo, Zimbabwe. The technique was combined with ground-penetrating radar (GPR) to map municipal sanitary landfills in the city of Gualeguaychú in the Southern Entre Ríos Province, Argentina (Pomposiello et al., 2012). The method, in theory, can also be used in utility detection or Subsurface Utility Engineering (SUE). SUE applies technology to accurately identify and map underground utilities in the early phase of the development of a project (Anspach, 2002). For the construction industry, the investigation of the subsurface is essential to avoiding unforeseen conditions that may cause project delays (Alel et al., 2015). From the work of Vickery and Hobbs (2002) subsurface conducting pipes can either be a target or noise in geophysical surveying indicating the potential

of the method to help investigate the subsurface for buried metallic pipes because metallic pipes are good conductors of electric current. Consequently, conducting pipe causes a strong response in the electrical geophysical survey, and the signature is well defined in some techniques (Vickery & Hobbs, 2002). Therefore, electrical resistivity was deployed for metallic pipe detection because of the method's ability to detect materials with different electrical properties. It was expected that, the subsurface conducting pipe causes a reduction of resistivity from the background value and reduces the resistivity values by about 60% (Vickery & Hobbs, 2002). For a dipole-dipole array, the resistivity is reduced when the pipe is between the dipoles and gradually increases away from the dipoles according to Vickery & Hobbs (2002).

1.1.3 Seismic Refraction Tomography

Seismic refraction tomography (SRT) can be used in investigating shallow levels of the subsurface and it is an imaging technique, which applies the same basic principle as conventional refraction shooting, except that more shots are fired before the first geophone, at each geophone point, and beyond the last geophone). It can resolve the velocity gradient, define lateral velocity changes, and may be applied in settings where conventional refraction techniques fail, such as areas of compaction, karst, and fault zones (Zhang & Toksöz, 1998). The method is increasingly used on a small-scale mapping of near-surface, mainly site investigation and it is a powerful tool to visualize subsurface layers. Azwin et al. (2013) applied seismic refraction to determine four layers with different velocities buried in the subsurface during a site investigation at Jalan Sahabat, Kaki Bukit, Perlis, Malaysia. Two-dimensional seismic refraction tomography was also deployed by Avalos et al. (2016) to map the bedrock topography beneath Hallsands beach in southwest Devon, United Kingdom. The constant use of this method tells how Seismic refraction tomography with time has become quite eminent in the geotechnical and civil investigation and the method together with Multi-Channel Analysis of Surface Wave (MASW) is described by Araffa et al. (2014) as the ‘‘work-horse’’ of engineering geophysics.

1.1.4 Multi-channel Analysis of Surface Waves Method (MASW) and Vs30

Multichannel Analysis of Surface Waves (MASW) is a fast, low-cost non-invasive seismic exploration method employed to determine near-surface shear wave velocity profile along with its depth, by analyzing horizontally traveling Rayleigh waves (Olafsdottir et al., 2018; Taipodia et al., 2020). MASW profiles are used in the interpretation of lithology, structural features, rock material quality, and geotechnical parameters. These results are very useful for foundation studies, environmental engineering, geotechnical investigations, and other civil engineering purposes. Abudeif et al. (2019) used MASW to delineate lithology and determine the geotechnical and engineering properties of the soil for foundation purposes.

Shear-wave velocity (VS) is a well-known parameter for evaluating the dynamic properties of soils (Martin & Diehl, 2004). Particularly, the time-averaged shear-wave velocity from the surface to the depth of 30 m (VS30) is an important parameter significant for seismic hazard analysis (Borcherdt, 1994; Volti et al., 2016). This parameter serves as a proxy for ground amplification and can help measure how the ground would respond to earthquakes or seismic events.

The history of seismic activities in southern Ghana is well established in the literature (Amponsah, 2004; Junner& Bates, 1941; Quaah, 1982). Major earthquakes have been recorded in the past; Elmina in 1615, Axim in 1636, and the well-known Accra earthquake in 1939 which recorded a magnitude of 6.5 according to Amponsah (2002). These seismic activities that dominate Ghana's southern part have been attributed to the St. Paul's and Romanche transform-fracture systems (Kutu, 2013) in the Atlantic ocean, and Ahulu et al. (2018) used a probabilistic approach to list the study area as a high-risk seismic hazard zone. Consequently, the effect of seismic energy on the study area must be well understood as an indicated by Nortey et al., (2018), a large part of Accra is situated on a complex distribution of shallow soft soils, which have the greatest potential to greatly intensify seismic waves and inflict harm.

2.0 Study Area and Geology Setting

2.1 Site Location

The study area is at the southwestern side of the main Commonwealth Hall building of University of Ghana. It is found between the geographic coordinates; (5° 39' 1''N, 0 11' 38''W), (5° 39' 1''N, 0° 11 34W) (5° 38' 58''N, 0 11', 38''W) and (5° 38' 58''N, 0 11'' 34). The site is generally sloppy and exposed service line valves and underground service utilities supplying water to the University of Ghana and its surrounding can be seen. Fig. 2. 1 and Fig. 2. 2 show a picture and a site plan of the site respectively.

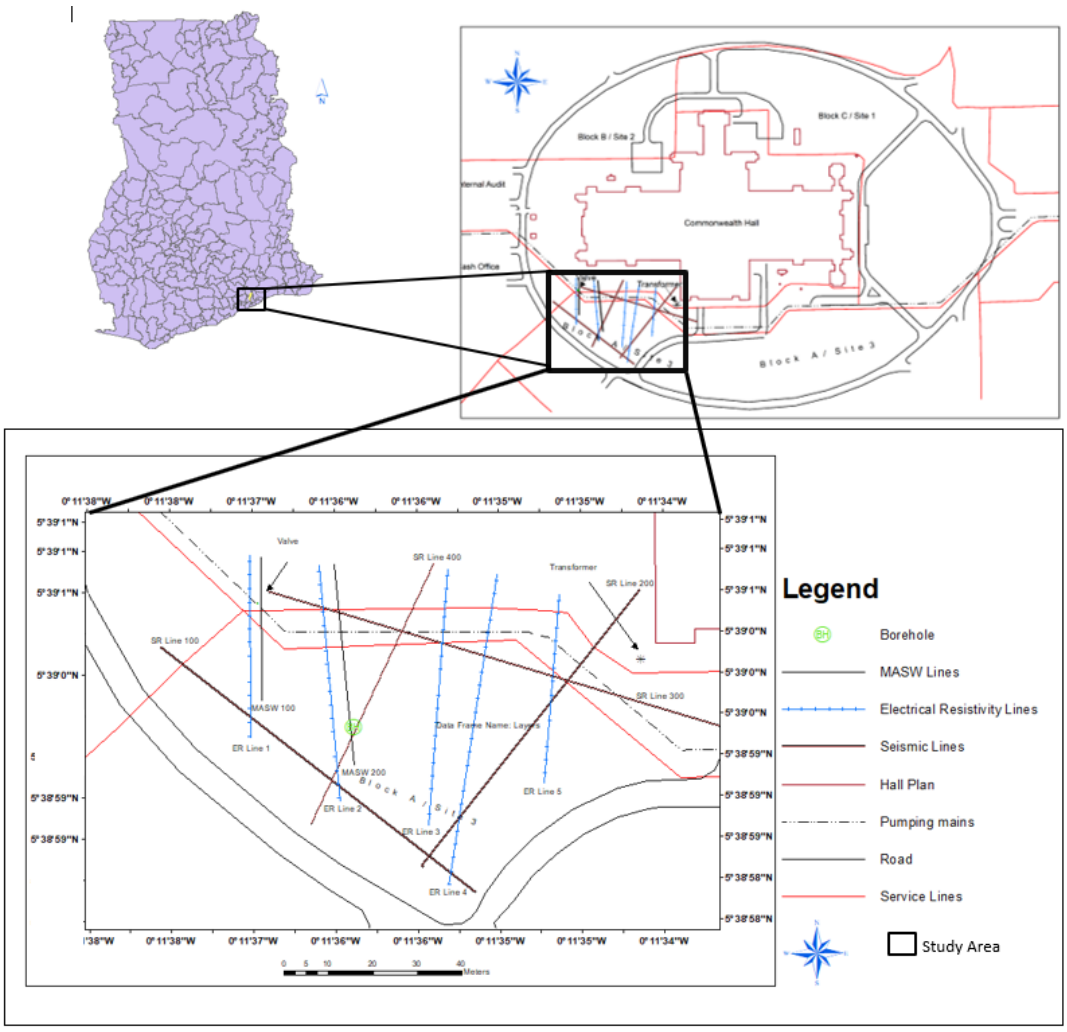

Fig. 2. 1: Map showing the location

Fig. 2. 2: Image of the construction site

2.2 Geology of Study Area

Fig. 2. 3 is the local geologic map of the study area; University of Ghana (UG) and it sits on the Pan African Dahomeyides, a place that resulted as the product of easterly subduction of oceanic lithosphere (Agbossoumondé et al., 2004). Consequently, three formations were created namely; The Dahomeyan, The Buem (BSU), and the Togo Structural Unit (TSU). It is on the Togo structural unit that the study area falls. Ahmed et al. (1977) describe the TSU as cataclastic quartzites interbedded with phyllites. Exposures of quartzites that are typical of the TSU as described by Adjei and Tetteh (1997) to consist of quartz sericite-schists, phyllites, and chlorite schist quartzites (Fig. 2. 4) are seen in some parts of the study area. The rocks show some brittle deformation and a regionally pervasive sub-horizontal foliation which is in agreement with deformational features of the TSU that are described by Adjei & Tetteh, (1997) and (Osae et al., 2006).

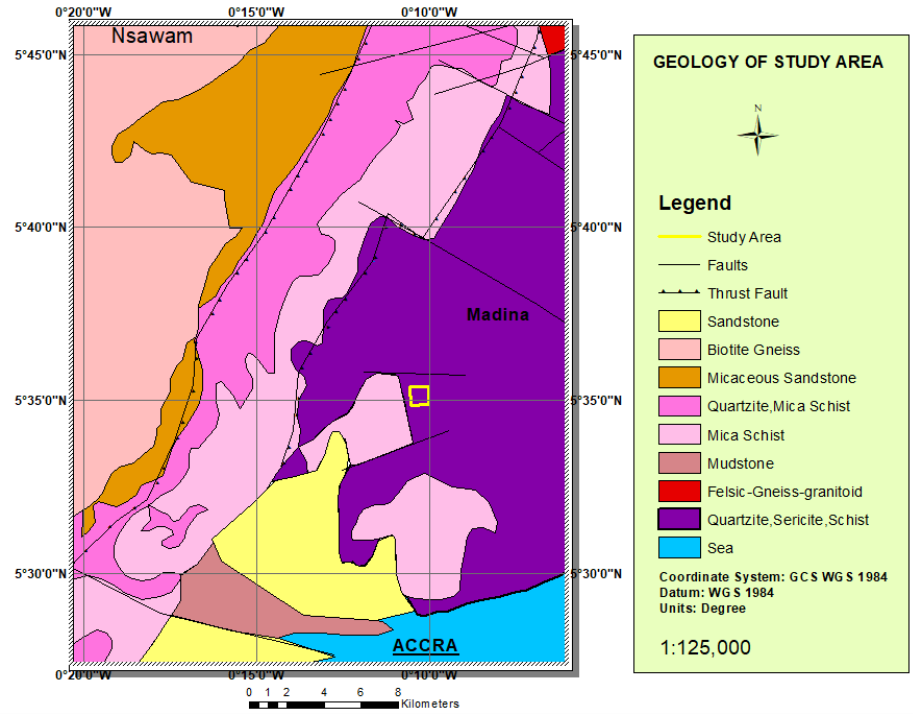

Fig. 2. 3:Local geologic map of the study area

Fig. 2. 4 : Example of a Quartzite exposure in the study area

3.0 Methodology

3.1 Electrical Resistivity Tomography

The site was investigated with SCINTREX SARIS` resistivity meter shown in Fig. 3. 1 .The instrument is a multi-electrode intelligent system with 25 electrodes.

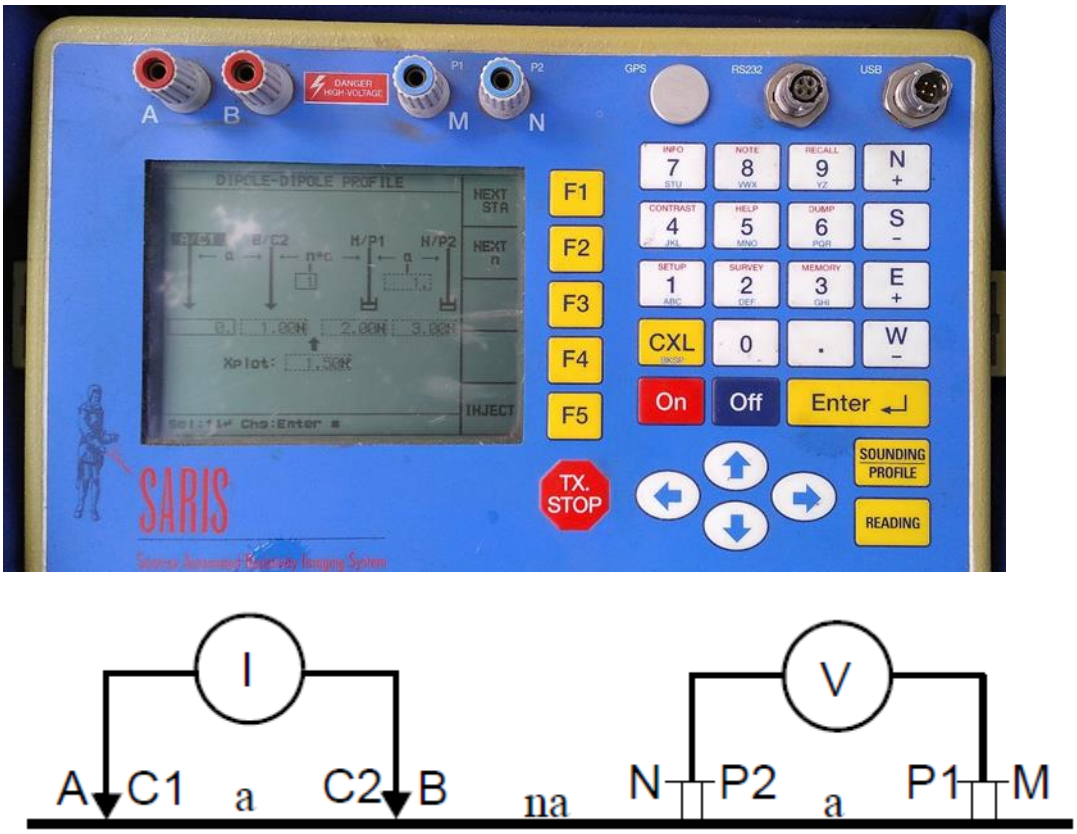

Fig. 3. 1: SCINTREX SARIS resistivity meter used in ER survey and a schematic diagram of the dipole-dipole array.

Measurements were made along five profile lines running North-south direction across the strike of some exposed metal pipes. Profile ER Line 1, ER Line 2, ER Line 3, ER Line 4, and ER Line 5 have a length of 61 m, 73 m,79 m,73 m, and 61m respectively. All the twenty-five (25) electrodes were arranged collinearly as in Fig. 3. 2 and an inter-electrode spacing of 1m was set up for the whole survey as measurements were made up to 10 levels(N-10). The role-along technique shown in Fig. 3. 3 was used to extend the survey line to cover the required length. Dipole-dipole resistivity

array was used for the entire survey because of the ability of the configuration to give a detailed image of the subsurface and also has high horizontal coverage.

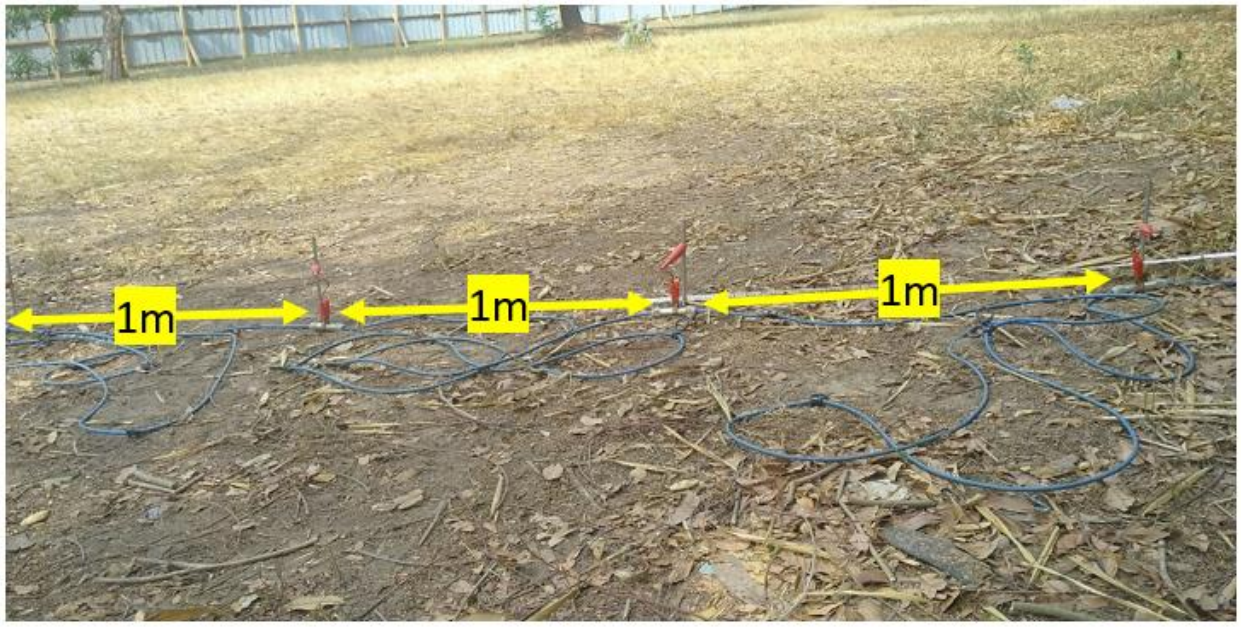

Fig. 3. 2 : Arrangement of electrodes for resistivity surveying

'

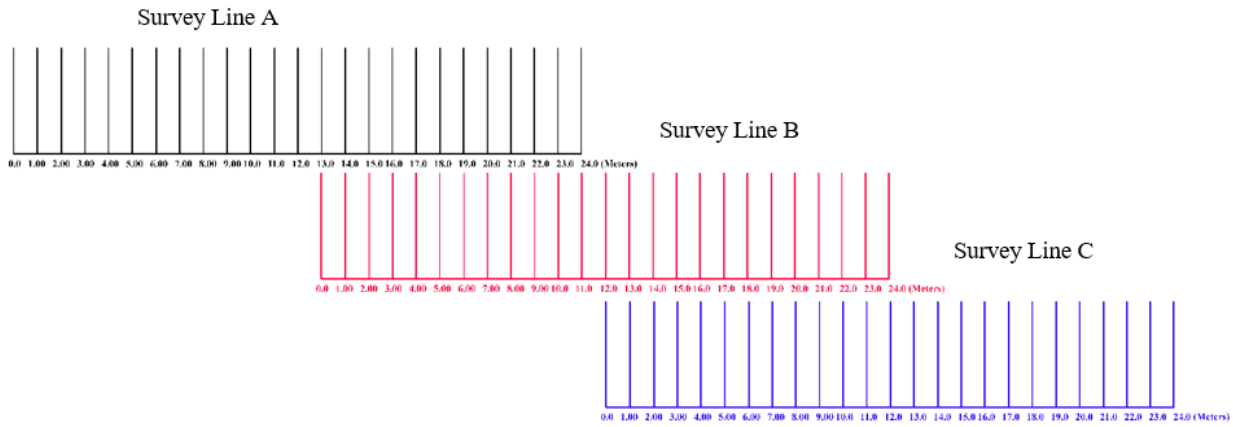

Fig. 3. 3 : ERT roll-along used in acquiring resistivity data

3.1.1 Data Processing and Inversion

Data was inverted with ZondRes2D inversion package using the smoothness-constrain least square interpolation method. A total of 4 iterations were enough to produce a reasonable resistivity model

because iterations usually converge between 4 to 6 for the least constrain inversion technique (Loke,2013). A total of five electric tomographic images were produced from the resistivity data and the corresponding instrument sensitivity pseudosections were also produced.

3.2 Seismic Refraction Tomography

3.2.1 Data Acquisition

Four seismic refraction surveys were made with the Smartseis TM which is made up of 24 channel seismographs connected to an eighteen-channel geophone with a frequency of 4.5 Hertz. The survey was made such that, two lines trend from North-South and the other East-West. Seismic energy was generated with a 10kg hammer impacted on a steel plate as multiple shots were made and the signals were stacked to increase the signal-noise ratio. A forward, reverse and two (2) split-spread shots were made for all surveys. Fig. 3. 4 is a diagram of how typical survey shots were made along a survey line.

Table 3. 1 also shows a summary of shot positions during data acquisition.

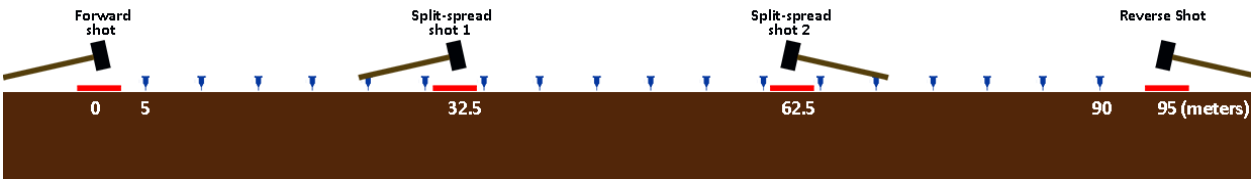

Fig. 3. 4 : Survey design of seismic refraction activity at the study area.

Table 3. 1 **:** Summary of data acquisition shot points for seismic refraction survey

Line	Start to End	Shot Points	Geophone spacing
SR Line 100	0 – 90	0m, 32.5m,62.5m,95m	5m
SR Line 200	0 – 85	0m, 27.5m,57.5m,85m	5m
SR Line 300	0 – 105	0m, 37.5m,67.5m,105m	5m
SR Line 400	0 – 68	0m, 22m,46m,68m	4m

3.2.2 Data Processing and Inversion

The first arrival times of P-waves were identified and picked on the seismograms that were captured from the 18 geophones as shown in

Fig. 3. 5 .

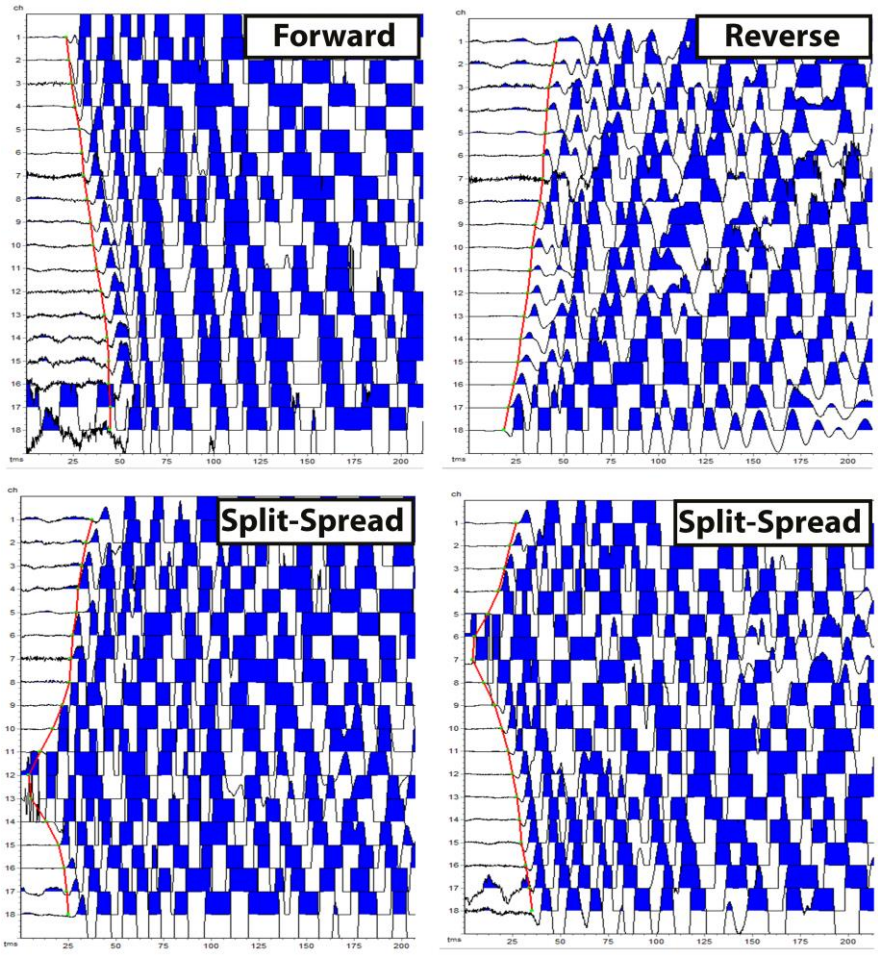

Fig. 3. 5 : A typical seismogram showing first arrival picks for seismic refraction data

The first arrival picks were inverted in ZondST2D with the Smoothness constraint algorithm which is based on the least square method and Jacobian matrix partial derivatives. Ten iterations were made on the data to achieve the best with a lower root mean square error. The robust weighting scheme was also applied to correct any inherent data with higher deviations.

3.3 Multi-Channel Analysis of Surface Waves

Surface wave data were collected using SmartSeis TM 24 Channel Seismograph connected to twelve (12) 4.5 Hertz vertical geophones. Data were collected on 2 lines, namely MASW 100 and MASW line 200 with both lines trending north-south of the study area. Surface waves (R-waves) were generated with a hammer on a steel plate of dimensions 300mm by 300mm. The vertical geophones were arranged 1m apart and shots were taken.

Fig. 3. 6 is a diagram showing how surface wave data was acquired.

Fig. 3. 6 : Survey procedure of MASW data acquisition

3.3.1 Data Processing

The SEG-Y data files obtained from the seismographs were processed and analyzed with ZondST2D software which comes with an MASW Module for surface wave processing. A dispersion image was generated from all the seismic records and the fundamental-mode dispersion curves were extracted . The 1D sections from all shot points were stacked together to produce a 2D section. The computed depth, Vs and Vs30 values were extracted to an Excel spreadsheet for analysis.Some trace records of MASW Line 100 and MASW 200 are shown in Fig. 3. 7

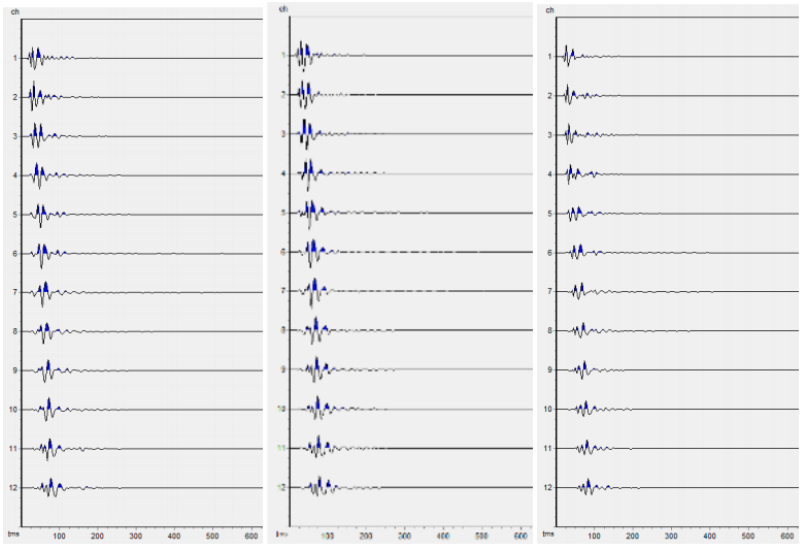

Fig. 3. 7 : Some trace records of MASW survey

The average shear wave velocity for the top 30 m of soil is referred to as VS30 according to (Kanlı et al., 2006) and it is a significant parameter for evaluating the dynamic behavior of soil was analyzed for MASW 100 and MASW 200. A Vs 30 profile was also produced from the Vs30 values by plotting the offset distance against shear wave velocities at 30m depth.

4.0 RESULTS AND DISCUSSION

4.1 Electrical Resistivity Tomography

Several low resistivity anomalies that may be signatures of the buried metallic pipes in the study area were detected on all the acquired electrical resistivity tomographic images. Fig. 4. 1 shows the electrical resistivity tomography of all survey lines of the study area. From ERT Line 1, about 13 low resistivity anomalies labeled A to M are identified. ERT Line 2 also shows about sixteen (16) low resistivity anomalies labeled A to Q, about 13 low resistivity anomalies labeled A to J are detected on ER Line 3, about sixteen (16), low resistivity anomalies are also identified on ERT Line 4 and 16 low resistivity anomalies are present on ERT Line 5 labeled A to P.

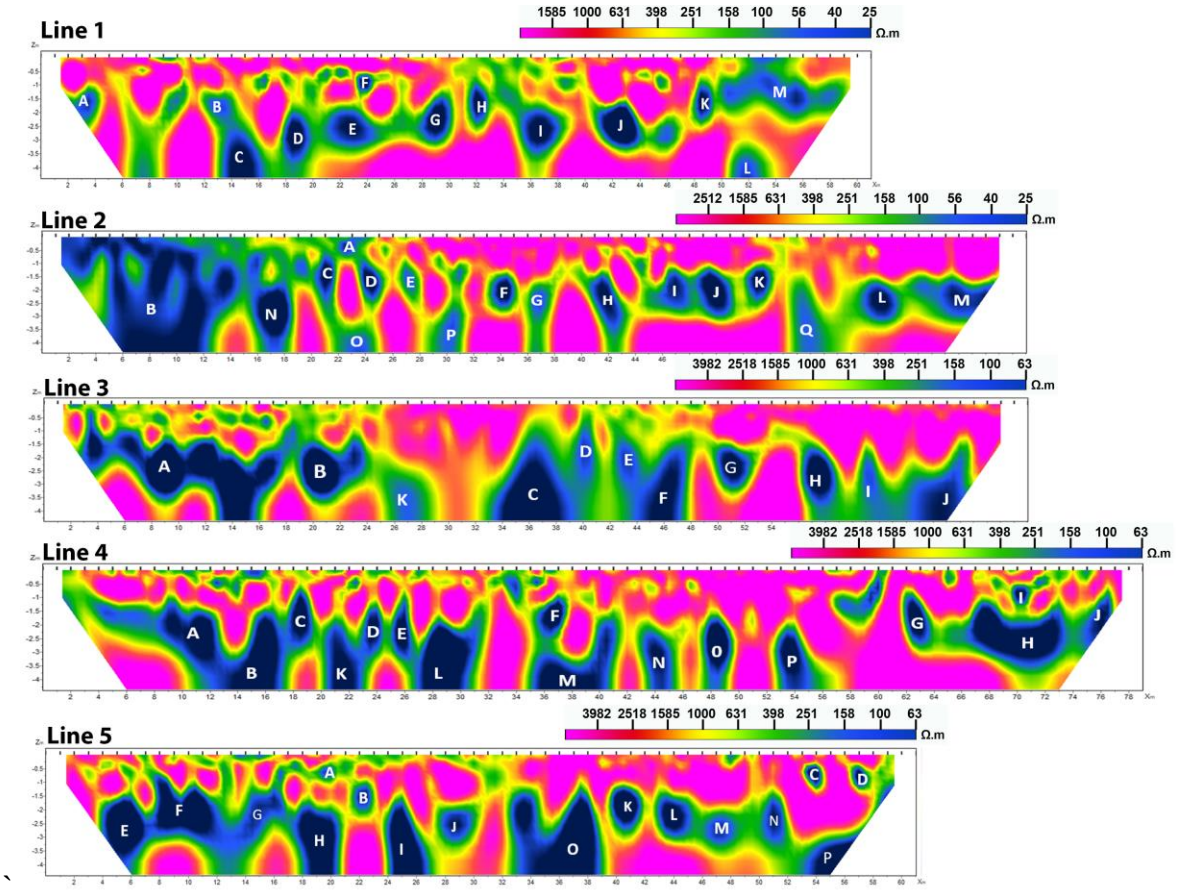

Fig. 4. 1 : Resistivity tomography of all the survey lines completed at the study area

4.1.1 Sensitivity Pseudosections Of Resistivity Instrument

The anomalies mapped at the subsurface occur at regions where the resistivity instrument is not equally sensitive, that is since electrodes are planted at the surface, the sensitivity of the resistivity instrument decreases at depth, and the sensitivity pseudosection in Fig. 4. 2 shows the sensitivity variation of the ground. Instrument sensitivity was higher to a depth of 1.5 meters and less sensitive at a depth of about 3.5 meters.

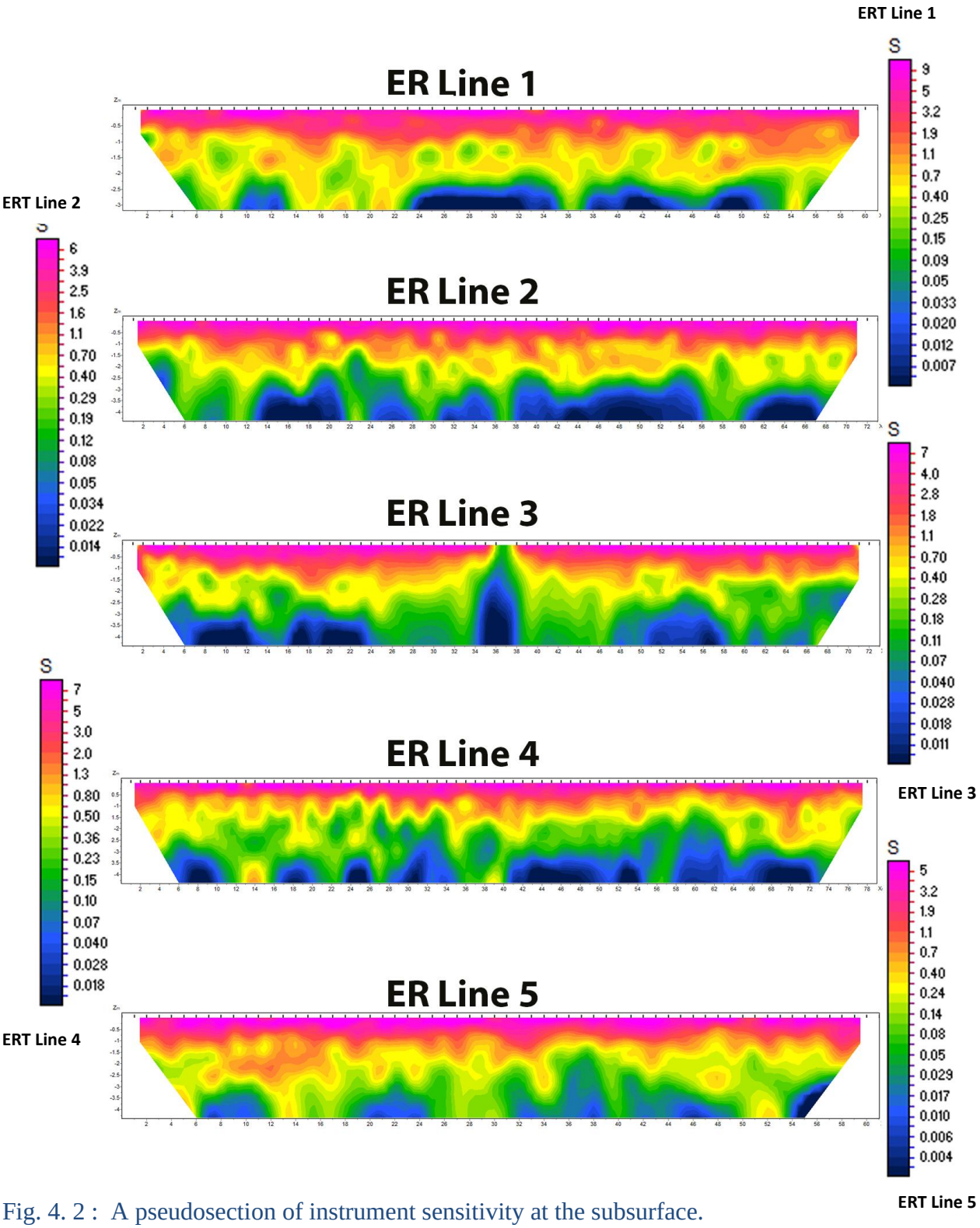

Fig. 4. 2 : A pseudosection of instrument sensitivity at the subsurface.

The sensitivity peaudosection is combined with the resistivity pseudosections to produce a map as in Fig. 4. 2 and categorizes the low resistivity anomalies per the sensitivity regions to give a

highlight to anomalous body detected .About 13 positions have been marked for suspected metallic pipes on ERT Line 1, about sixteen (16) positions marked for ERT Line 2, 11 positions marked for ERT Line 3, 10 positions marked for ERT Line 4, and about sixteen (16) positions are marked for ERT Line 5.

Most low resistivity anomalies occur in regions of higher to moderate instrument sensitivity and the rest are distributed in the region of lower instrument sensitivity. On ERT Line 1, a single low resistivity anomaly is detected at a region of high instrument sensitivity, 8 low resistivity anomalies are detected at moderate instrument sensitivity and 5 low anomalies occur at low instrument sensitivity. ERT Line 2 shows 2 low resistivity anomalies in a region of low instrument sensitivity, 8 low resistivity anomalies in a region of moderate instrument sensitivity, and 12 low anomalies in a region of high instrument sensitivity.ERT Line 3 has all anomalies within a moderate and higher region of instrument sensitivity, 7 low resistivity anomalies are detected at a moderate region of instrument sensitivity and 12 are detected at a region of higher instrument sensitivity. On ERT Line 4, 2 low anomalies were present at high instrument sensitivity region, 9 at moderate sensitivity region, and 7 are present at high instrument sensitivity region. The final ERT Line 5 has a single low resistivity anomaly at the highest instrument sensitivity region, 5 low anomalies at the moderate sensitivity region, and 4 low anomalies at the high sensitivity region.

Table (4.1) and Fig. Fig. 4. 3 below show a summary and a map of low anomalous bodies at different sensitivity regions where utility pipes may be distributed in the study area.

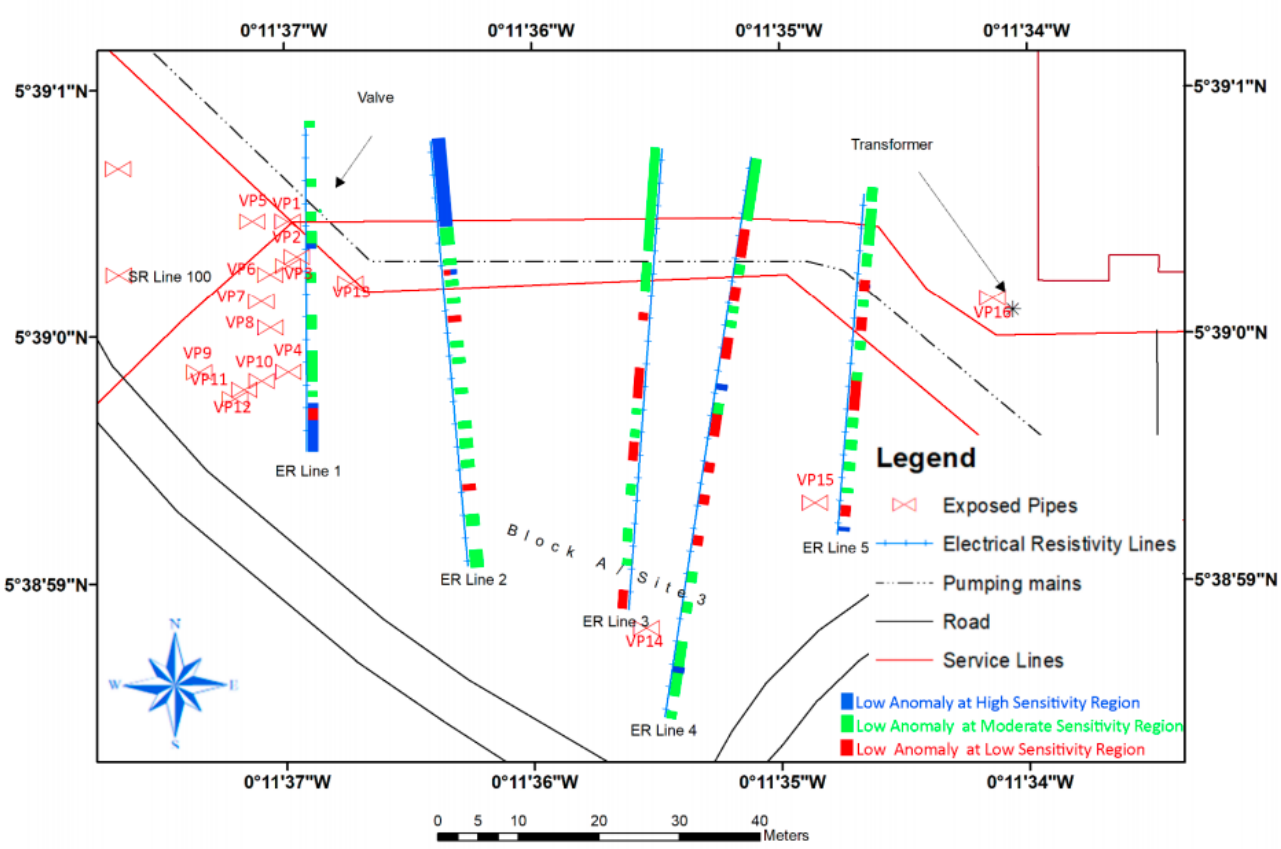

Fig. 4. 3 : Map showing low resistivity anomalies at different instrument sensitivities.

Table 1 : Summary of low resistivity anomalies at different instrument sensitivity regions

Resistivity Lines	Low Anomalies in high sensitivity region	Low Anomalies in moderate sensitivity region	Low Anomalies in low sensitive region
ER Line 1	1	8	1
ER Line 2	2	12	3
ER Line 3	0	7	4
ER Line 4	2	9	7
ER Line 5	1	10	4

4.2 Resistivity Slice (N-1 N-3 N-7 AND N-10)

Generally, resistivity measurements become smaller as a function of depth for the depth slices produced at the site.These slices also suggest that resistivity anomaly distribution in the northwestern are lower and becomes larger towards the southeastern area. The pockets of lower and larger resistivity anomalies, displayed along the electrical resistivity profile lines are present probably due to the artifacts or bullseyes that are normally associated with the IDW interpolation method. (Nusret & Dug, 2012). These artifacts occur as circular or concentric features as in Fig. 4. 4 and are associated with the IDW interpolation due to equal values localized around a point. Resistivity values recorded for all the slices range from 7000 Ohm. m to about 10 Ohm, with the high anomalies mostly at the southern part of the study area,, Labelled HR in Fig. 4. 4. The highest resistivity values are confined to the two shallow resistivity slices 1 and 3. The Moderate resistivity values range between 900 Ohm. m and 3000 Ohm. m and generally occur at the middle section labeled as MR1 in Fig. 4. 4 . Slice 1 which forms the shallowest part of the study area suggests a generally higher resistivity surface. Slice 3 represents about 1.25 m of the subsurface and resistivity anomalies observed on this slice are similar to the anomalies observed in slice 1 but with the emergence of enhanced areas of low resistivity anomalies especially at the northwestern corner labeled in Fig. 4. 4 as LR2A.Slice layer 7 represents a depth of about 2.9 m and significant changes appear in resistivity values compared to the resistivity of slice 1 and slice 3. Resistivity values at slice 7 and slice 10 experience a reduction in resistivity values as values drop to about 2000 Ohm. m; less than that of slices 1 and 3 . Low resistivity anomalies become more prominent and begin to extend to the southern part of the study area. The resistivity anomalies at slice 10, which represents about 4m of the subsurface are similar to anomalies on slice 7.

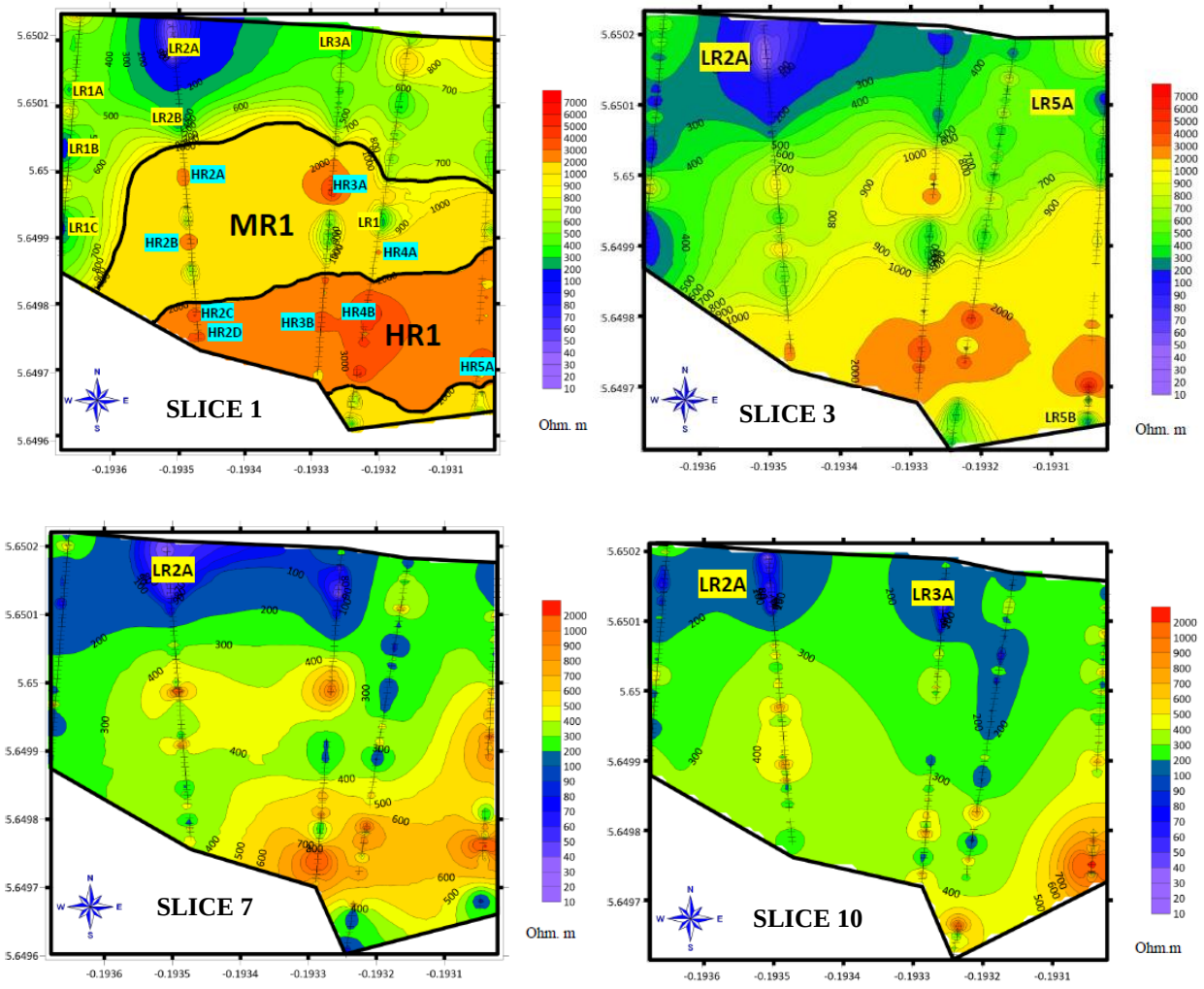

Fig. 4. 4: Showing the electrical resistivity distribution for the depth slices in the study area

Depth slices have been used to develop a geoelectric section of the study area and it is shown in Fig. 4. 5 and Fig. 4. 6. The area has been categorized into three (3) geoelectric sections, geoelectric sections with resistivity values less than 300 Ohm are prevalent in the northmost part of the study area. Section with a resistivity between 300 Ohm. m and 2000 Ohm. m occurs in the middle section and sections with values greater than 2000 Ohm. m are at the southmost part of the study area. Lower resistivity anomalies become prominent as the depth of measurement increases. Reduction of resistivity values with depth may be due to the presence of metallic pipes that superimpose their effects in the form of noise and reduce the resistivity values recorded according to Vickery

& Hobbs (2002). This phenomenon may be possible because, as measurements are taken closer to the buried pipes, their noisy effect is gradually felt reducing resistivity values within that region.

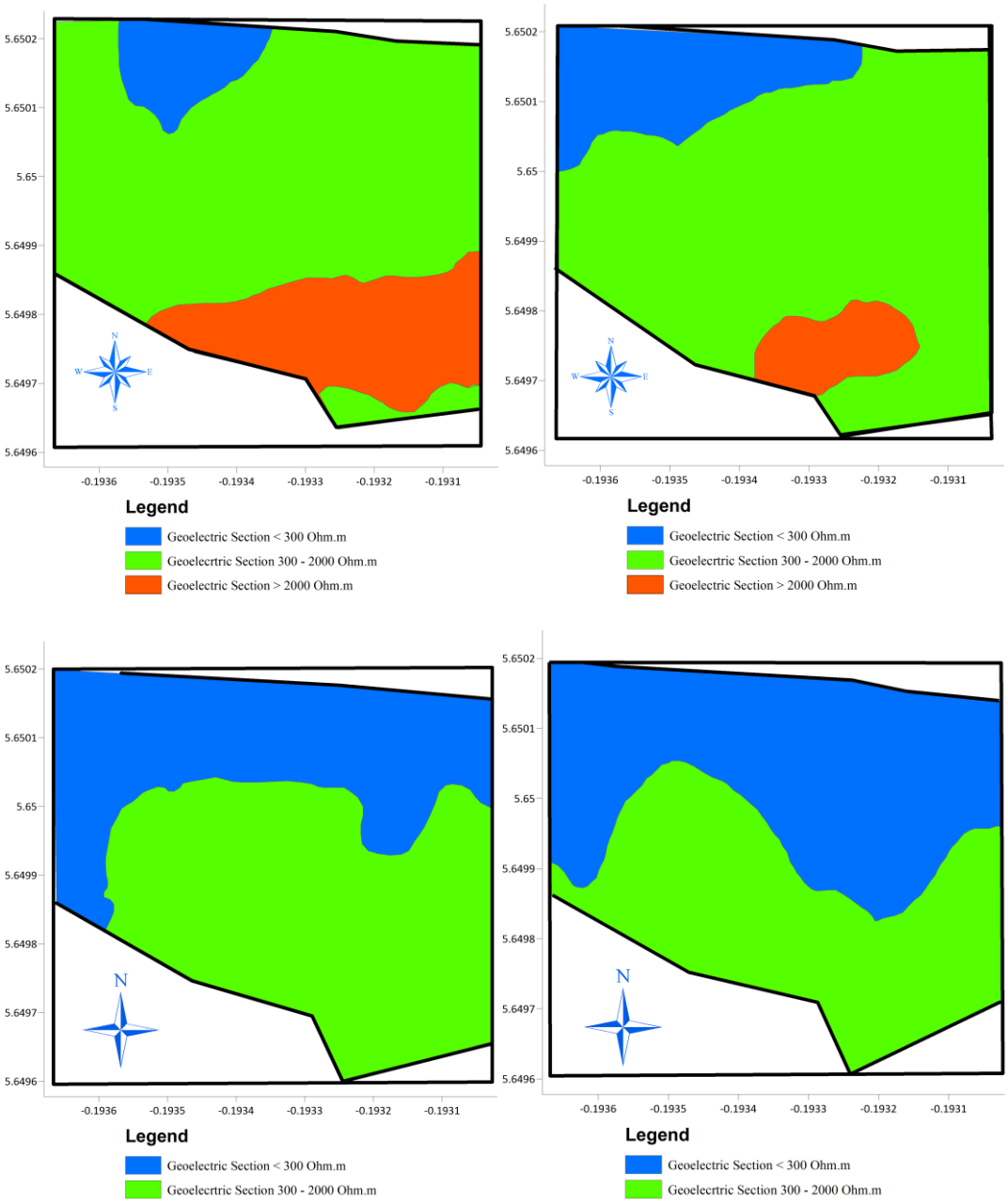

Fig. 4. 5 : Geoelectric sections developed from four resistivity depth slices of the study area

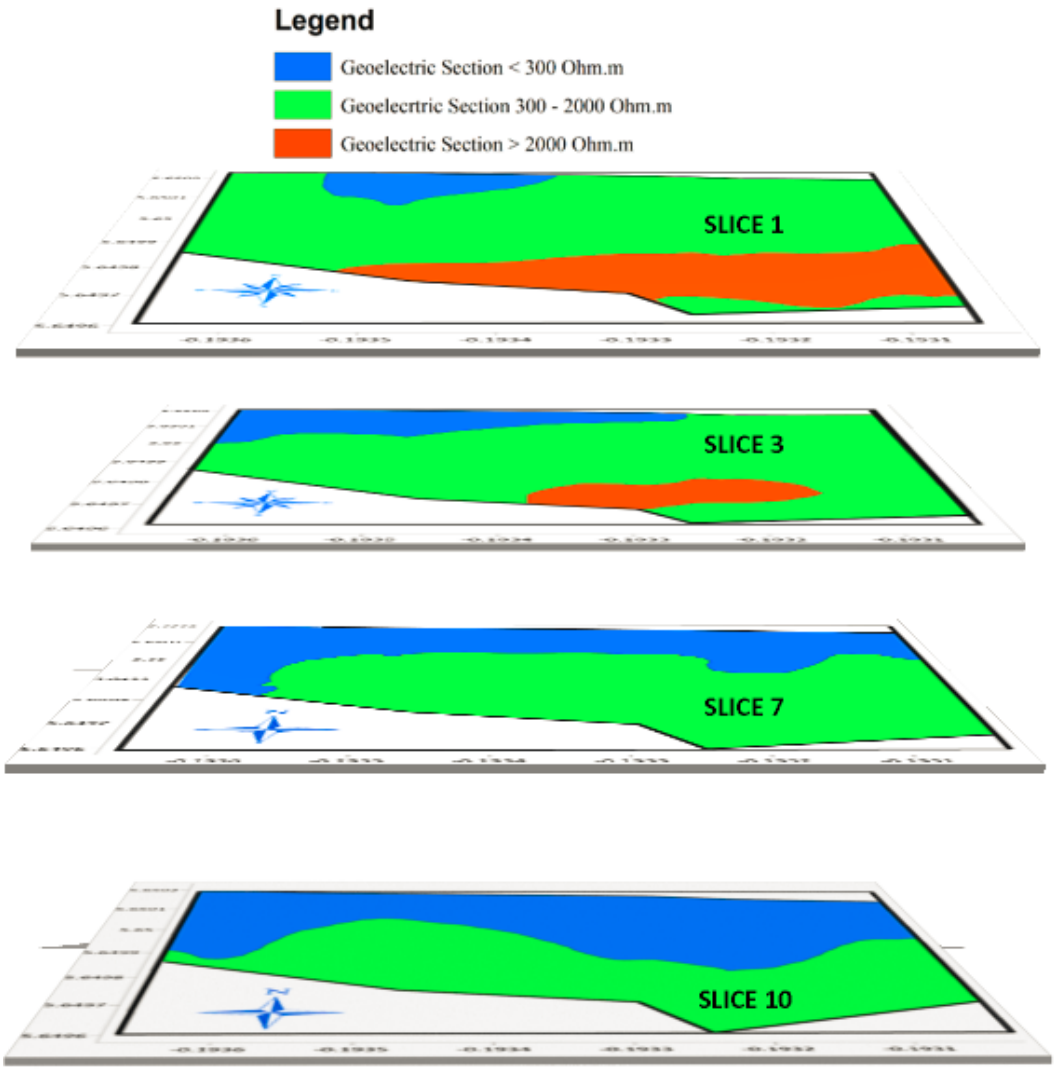

Fig. 4. 6 : A 3D impression of the geoelectric section of the subsurface of the study area.

Geoelectric sections of resistivity values of less than 2000 Ohm. m may represent the laterites as these values are consistent with the 800 Ohm. m to 1500 Ohm. m range of resistivity values reported by Reynold (2011) for lateritic materials. Similarly, the resistivity values greater than 2000 Ohm. m seems to represent the quartzites according to the geology of the area.

4.7 Seismic Refraction Tomography

4.7.1 SRT Line 100

The length of SRT Line 100 is 105m and three velocity layers that run from east to the west are delineated as shown in Fig. 4. 7. The depth of reach of this survey line is about 30m. The first velocity layer A has a thickness of about 3m, the second layer B has a thickness of about 8m, and the third layer C is at a depth of about 10 m. The velocity of the top layer is about 1.200 km/s, followed by the second layer with a velocity of about 2.200 km/s, and the third layer C with a velocity of about 3.200 km/s.

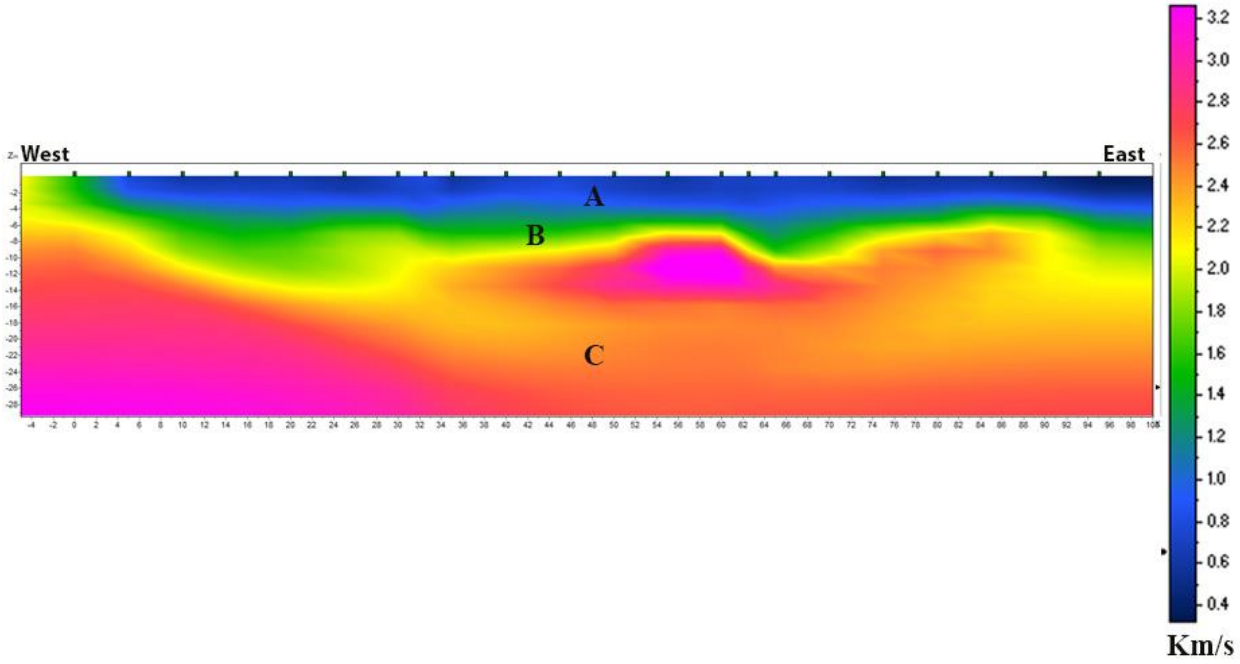

Fig. 4. 7: Seismic refraction tomography SRT Line 100

4.7.2 SRT Line 200

Fig. 4. 8 also represents the seismic refraction tomography of SRT line 200 and the first velocity layer labeled M has a thickness of about 5m. The second layer N has a thickness of 4m and the third layer O is at a depth of about 10m. The first layer has a velocity of about 1.000 km/s, with the second and third layers having a velocity of about 2.000 km/s and 3.200 km/s respectively.

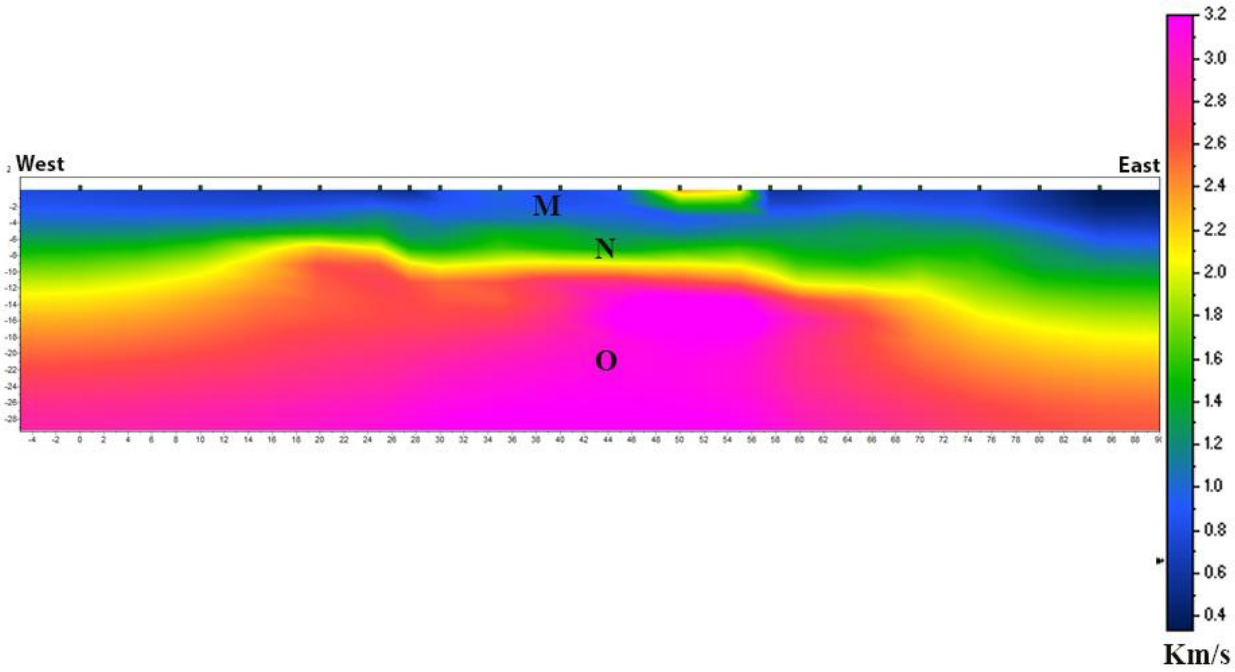

Fig. 4. 8: Seismic refraction tomography SRT Line 200

4.7.3 SRT Line 300

SRT Line 300 as shown in Fig. 4. 9, indicates that the first layer X has a velocity of about 1.400 km/s and a thickness of about 5m. The second velocity layer Y has a velocity of about 2.400 km/s with a thickness of about 6m and the third velocity layer Z has about 3.600 km/s.

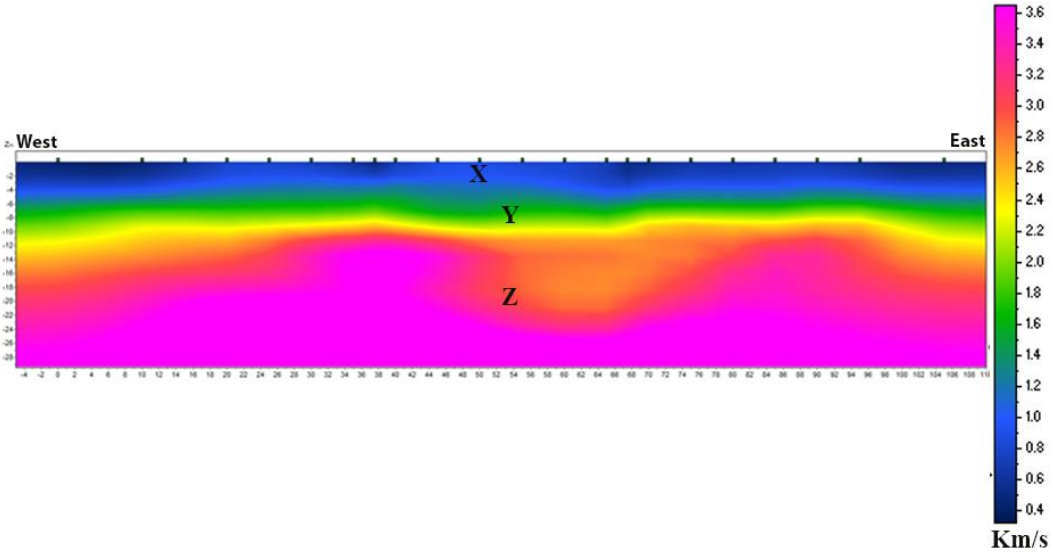

Fig. 4. 9: Seismic refraction tomography SRT Line 300

4.7.4 SRT Line 400

SRT line 400 also suggests three velocity layers, the first velocity layer Q has a thickness of about 3m and a velocity of about 1.100 km/s. At a depth of about 4m, the second layer R is encountered with a velocity of about 2.400 km/s. The third velocity layer S labeled in Fig. 4. 10, has a velocity of about 2.700 km/s, and its encountered at a depth of about 6m and extends to a deeper. A borehole drilled to a depth of 5.15m on SRT Line 400 indicates that the subsurface is made of laterites, fragmented quartzites, and weathered quartzites.

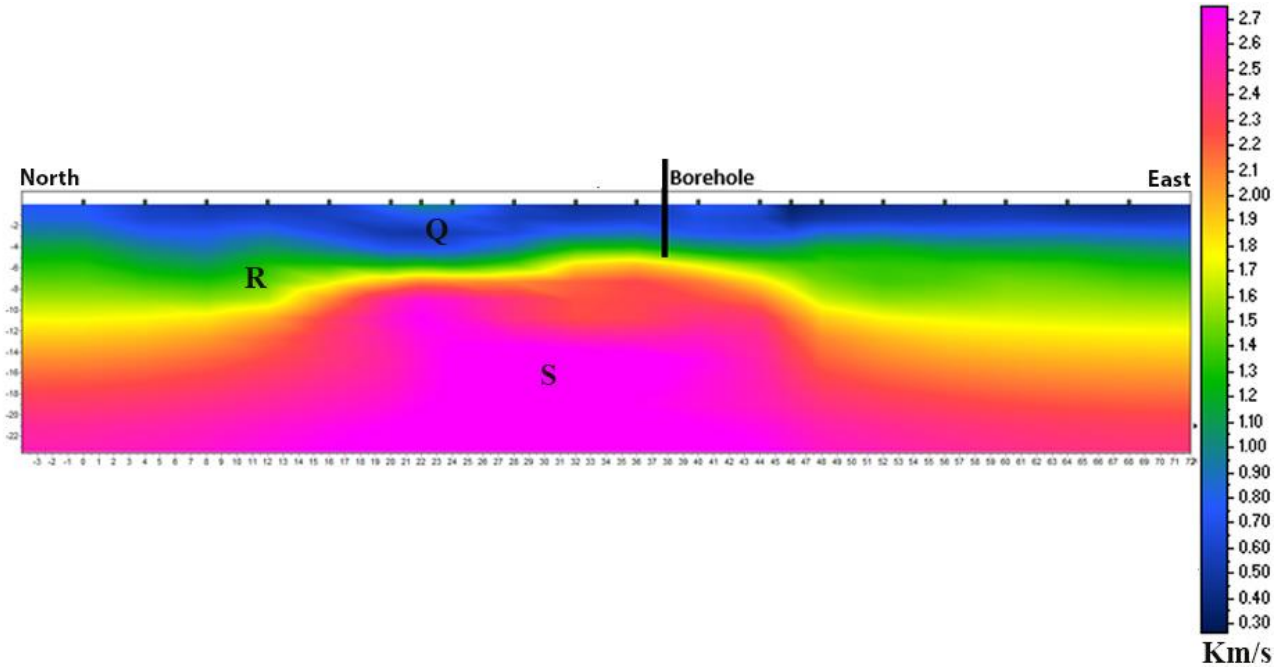

Fig. 4. 10 : Seismic refraction tomography SRT Line 400

4.8 SRT DISCUSSION

4.8.1 SRT Line 100

The four seismic tomographies (SRT Line L100, L200, L300, and L400) generated from seismic refraction tomography suggest that there are three velocity layers at the subsurface to a depth of about 30 m. The average depth of the bedrock is estimated to be about 10 m according to the four seismic refraction images.

Fig. 4. 11 shows the velocity model of the subsurface layers according to SRT Line 100 which runs from East to West of the study area. The velocity of the first layer is estimated to be less than

1.300 km/s. The second layer has an estimated velocity between 1.300 km/s and 2.000 km/s and the third layer which represents the bedrock is estimated to have a velocity between 2.100 km/s and 3.200 km/s and occurs at a depth of about 6m.

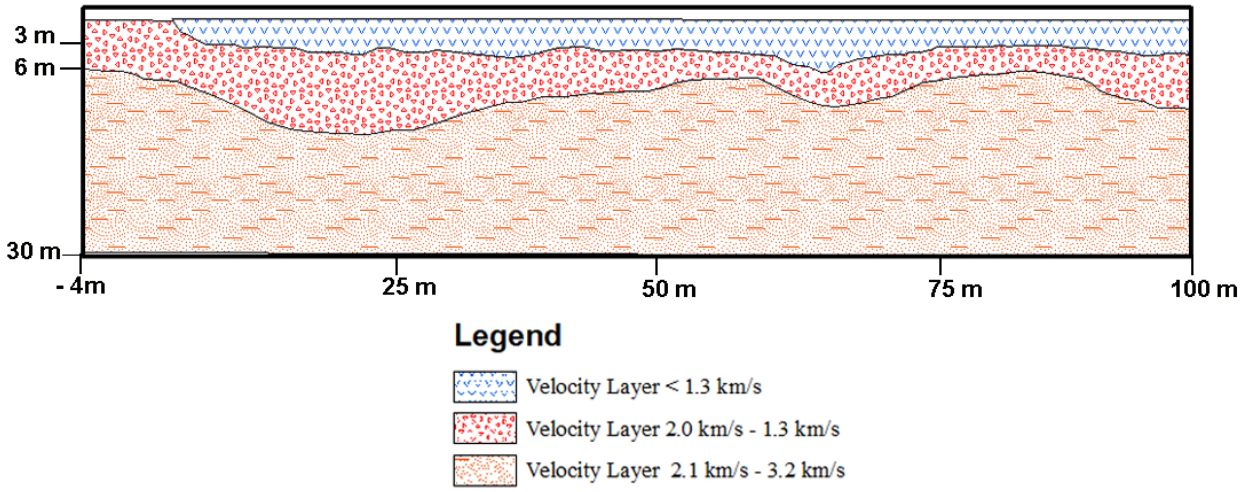

Fig. 4. 11 : Velocity layer model of SRT Line 100

Fig. 4. 12 also represents the velocity model according to SRT 200 which runs from North to South of the study area. The model also suggests that three velocity layers are present. The first layer has a velocity of less than 1.100 km/s. The second layer has a velocity between 1.000 km/s and 2.000 km/s and the third layer has a velocity greater than 2.100 km/s.The bedrock on this survey line is estimated to be at a depth of 11m.

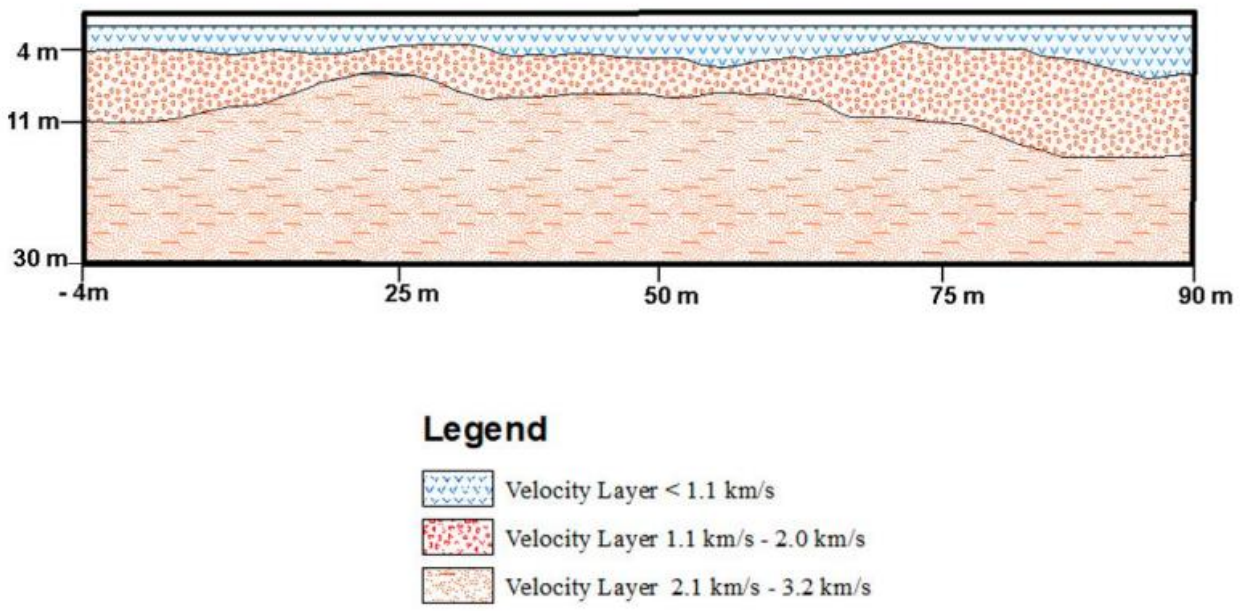

Fig. 4. 12: Velocity layer model of SRT Line 200

SRT Line 300

Fig. 4. 13 represents the velocity layer model according to SRT Line 300. Three velocity layers have also been identified. The top layer has a velocity of less than 1.400 km/s and a thickness of about 4 m, the second layer has a velocity between 1.400 km/s to 2.200 km/s with a thickness of 6 m, and the third layer which is the bedrock has a velocity between 2.300 km/s and 3.600 km/s and is estimated at a depth of about 11 m.

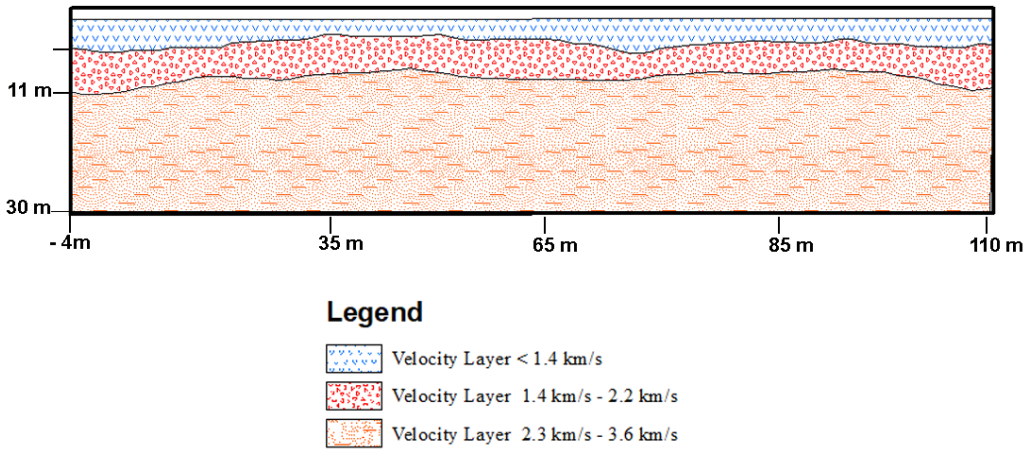

Fig. 4. 13: Velocity layer model of SRT Line 300

LINE 400

Fig. 4. 14 is the model for the interpreted layers of SRT Line 400. This tomography also suggests that there are three velocity layers buried in the subsurface. The first layer has a velocity of less than 1.000 km/s and a thickness of about 2 m, the second layer has a velocity between 1.000 km/s and 1.700 km/s with a thickness of about 8m. The third layer considered to be the bedrock at a depth of about 10 m has a velocity between 1.800 km/s and 2.700 km/s.

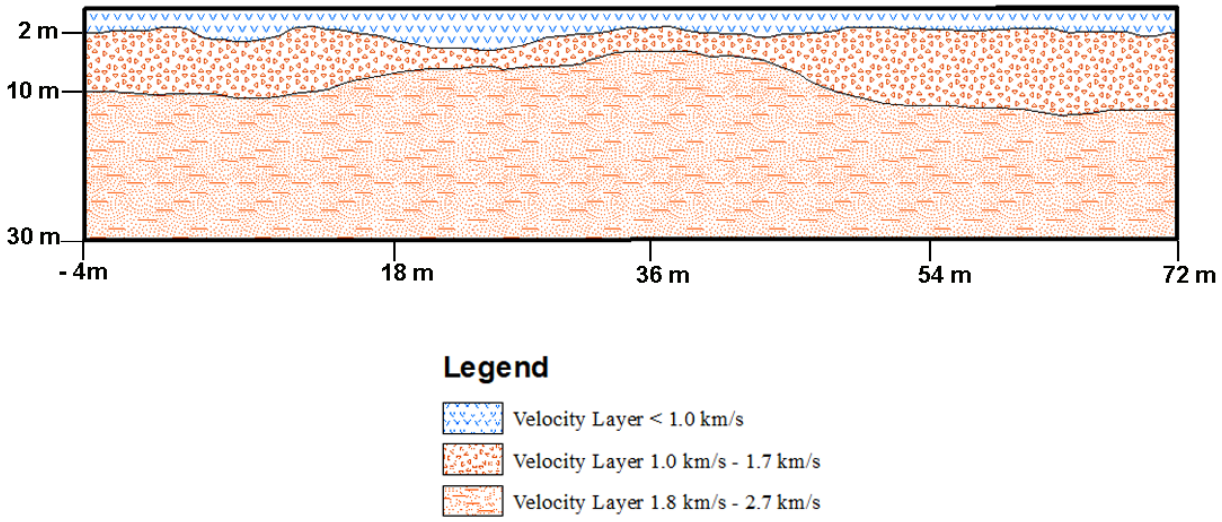

Fig. 4. 14: Velocity layer model of SRT Line 400

A borehole drilled to a depth of 5.15 m at SRT Line 400 revealed that the first 5.15 m depth consists of Lateritic material, quartz fragment, and weathered quartzite. Laterite, quartz fragment, and the weathered quartzite occurred at a depth of about 3 m, 3.9 m and 5.15 m respectively. Correlating these layers with the borehole report suggests that the three possible layers that are delineated by the seismic refraction tomography are the top lateritic layer with a velocity of about 1.400 km/s, quartzite fragments with a velocity between 1.400 km/s and 2.200 km/s, and weathered quartzite with a velocity of about to 3.200 km/s. According to Reynold (2011), laterite has a velocity between the range of 0.800 km/s to 1.500 km/s, suggesting that the top velocity layer occurring from the surface to a depth of about 3 m, delineated by SRT is consistent with the borehole report.

The fragmented Quartzites that form the second layer also seem to have their velocity reduced, and this reduction in velocity may be due to a deficiency in compactness of the quartz material due to fragmentation (Milsom, 2003).

According to Adjei and Tetteh (1997), the study area is underlain by Quartzites which are expected to have higher velocities in the range of about 5.960 km/s to about 6.090 km/s as estimated by Christensen and Stanley (2003), however the effect of weathering may have reduced the velocities of the Quartzites encountered at depth. Therefore the bedrock has been interpreted as possible quartzite formation. As indicated by Palmström (1996) velocities of the seismic wave in a rock body varies with the degree of weathering.

4.9 Vs30 RESULT AND DISCUSSION OF MASW 100 AND MASW 200

4.9.1 MASW 100

The average surface wave velocity at 30m, Vs30 of the study area is about 0.720 m/s. Vs30 increases generally from the northern part of the study area to the southern part. The lowest Vs30 value of 0.631 m/s is recorded at 10 meters of the MASW survey line and the largest Vs30 value of 1030 m/s is recorded at 32m of the MASW 100 survey line.

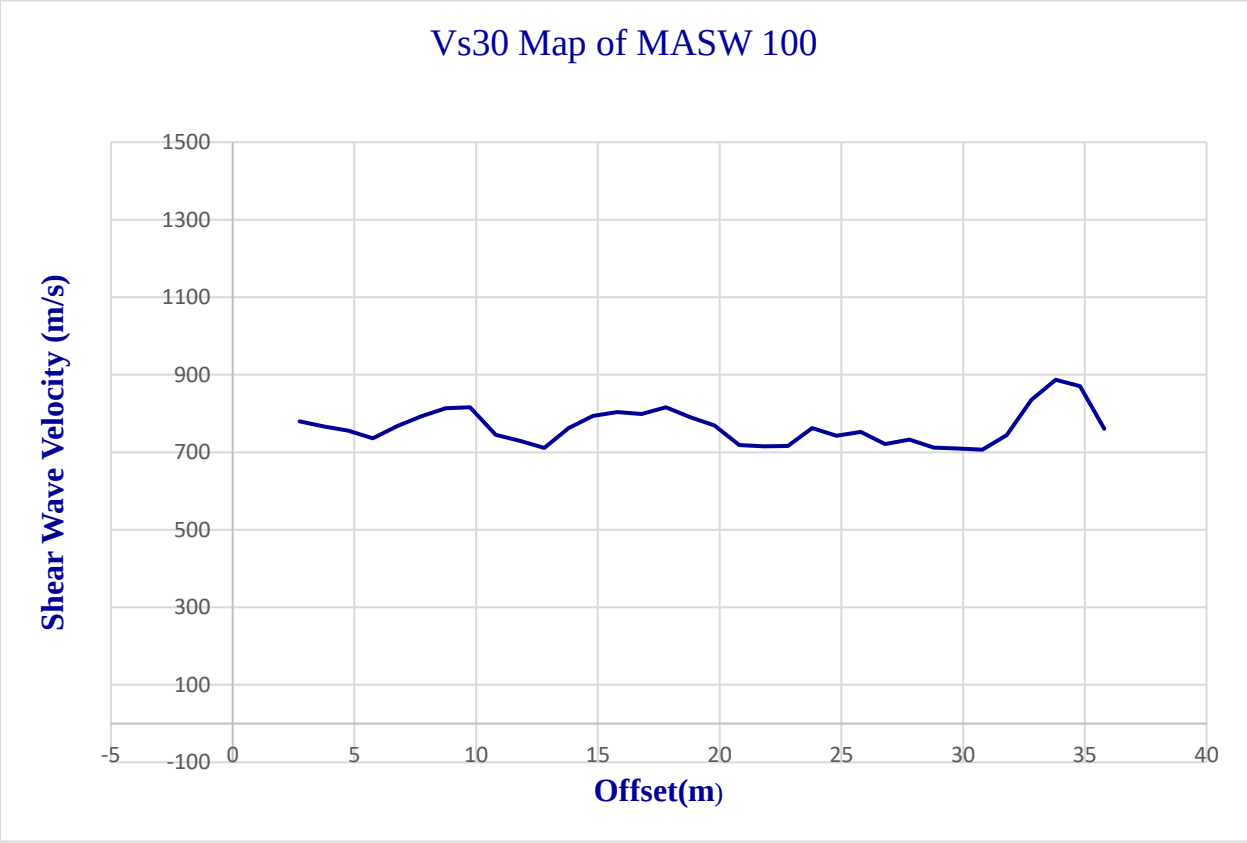

The average surface wave velocity at 30m Vs30 of the MASW survey line 200 is 761 m/s.Vs30 values fluctuate from the northern part of the MASW survey line 200 with the lowest value of 547 m/s and highest values of 842 at 17m and 37m respectively.

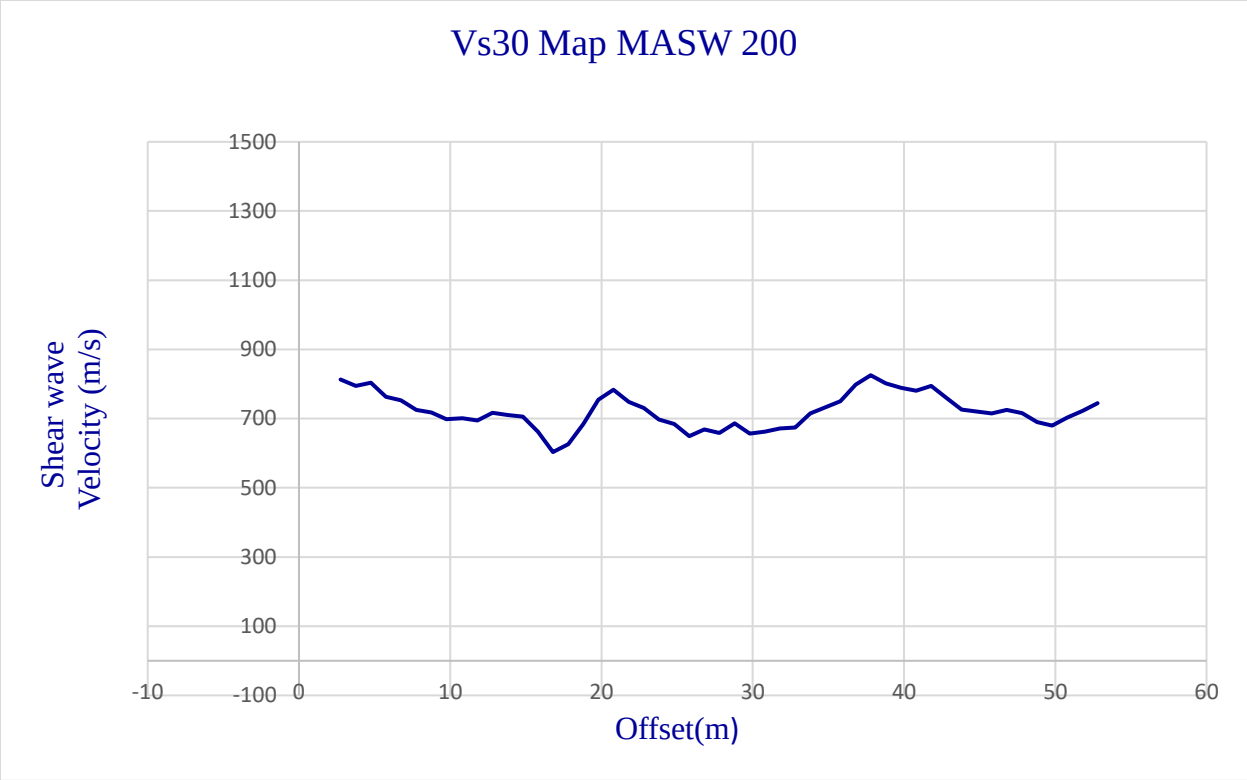

4.9.1.1 Discussion of VS30 Results

The Vs30 results of the study area suggest that subsurface geologic bodies at a depth of 30m have an average shear wave velocity between 0.720 Km/s and 0.760 km/s. The Vs30 between this range is classified as class C according to the NERHP (2003) site classification implying that the underlying subsurface material is a soft weathered rock material. Weathered materials can influence ground amplification or have a huge impact on earthquake site response during a seismic event (Davis, 1995; Steidl et al., 1996), this is because ground acceleration in weathered rocks may increase up to about 20% compared to unweathered rocks according to Rodri´ guez-Marek et al. (2001).

4.10 CONCLUSION

Three geophysical techniques have been used to investigate a proposed site for the construction of 5 story buildings for Commonwealth Hall of the University of Ghana in Accra. The aim was to apply electrical resistivity to map buried utility pipes and highlight the geoelectric sections of the area, apply seismic refraction to determine the prevailing subsurface velocity layers, delineate the depth of the bedrock and also use MASW to determine the class site of the study area.

Firstly, the electrical method has been used to detect points in the study area where suspected metallic pipes are located. The Electrical Resistivity Tomography detected about 71 low resistivity anomalies that may be the signatures from the metallic pipes. Six (6) of these signatures occur at the depths where resistivity instruments are most sensitive, 46 occur at where the resistivity instrument is moderately sensitive and 19 are located where the resistivity instrument has low sensitivity.

Secondly, Seismic Refraction has been used to image the subsurface and estimate the depth to the bedrock. Three velocity layers have been identified with the first layer of the recording an average thickness of about 4m and a wave velocity of less than 1.400 km/s. The second velocity layer has an average thickness of about 7m and a wave velocity between 1.400 km/s and 2.000 km/s. The average depth to the bedrock which is the third layer is estimated to be about 10 m and has a velocity between 2.300 km/s and 3.600 km/s. Borehole report from one of the seismic lines (SRT Line 400) suggests that the top layer to about 5.15m consists of a lateritic material, followed by quartzite fragments and a weathered quartzite.

The Vs30 which is a proxy for ground amplification during the earthquake has also been computed for the study area. The Vs30 value of the area is between 0.720 km/s and 0.762 km/s and this is classified as a C site, implying a soft weathered subsurface material.

Conflict Of Interest

The authors report no conflicts of interest. The authors alone are responsible for the content and writing of this article.

REFERENCES

1. Abudeif, A. M., Fat-Helbary, R. E., Mohammed, M. A., Alkhashab, H. M., & Masoud, M. M. (2019). Geotechnical engineering evaluation of soil utilizing 2D multichannel analysis of surface waves (MASW) technique in New Akhmim city, Sohag, Upper Egypt. Journal of African Earth Sciences, 157, 103512.
2. Adjei, A., & Tetteh, G. (1997). Deformational phases of the Togo series, Ho-Nyive-Honuta area, Ghana. Ghana Mining, 3(1), 1-9.
3. Agbossoumondé, Y., Guillot, S., & Ménot, R.-P. (2004). Pan-African subduction–collision event evidenced by high-P coronas in metanorites from the Agou massif (southern Togo). Precambrian Research, 135(1-2), 1-21.
4. Ahmed, S., Blay, P., Castor, S., & Coakley, G. (1977). Geology of Field Sheets 33, 59, 61 and 62. Winneba NW, Accra, SW, NW, and NE, respectively. Geological Survey.
5. Ahulu, S. T., Danuor, S. K., & Asiedu, D. K. (2018). Probabilistic seismic hazard assessment of southern part of Ghana. Journal of seismology, 22(3), 539-557.
6. Alabi, A., Adewale, A., Coker, J., & Ogunkoya, O. (2018). Site Characterization for Construction Purposes at FUNAAB using Geophysical and Geotechnical Methods. Materials
7. Alel, M. N. A., Saad, R., Abdullah, R. A., & Wei, L. I. (2015). Applicability of electrical resistivity tomography in subsurface utilities engineering. Jurnal Teknologi, 76(2).
8. Amponsah, P. E. (2002). Seismic activity in relation to fault systems in southern Ghana. Journal of African Earth Sciences, 35(2), 227-234.
9. Amponsah, P. E. (2004). Seismic activity in Ghana: past, present and future. Annals of Geophysics, 47(2-3).
10. Anspach, J. H. (2002). Standard guideline for the collection and depiction of existing subsurface utility data. Paper presented at the Pipelines 2002: Beneath Our Feet: Challenges and Solutions.

11. Araffa, S. A. S., Atya, M. A., Mohamed, A. M., Gabala, M., Zaher, M. A., Soliman, M. M., . . . Geophysics. (2014). Subsurface investigation on Quarter 27 of May 15th city, Cairo, Egypt 112
12. Auken, E., Pellerin, L., Christensen, N. B., & Sørensen, K. (2006). A survey of current trends in near-surface electrical and electromagnetic methods. Geophysics, 71(5), G249-G260.
13. Avalos, E. B., Malone, D. H., Peterson, E. W., Anderson, W. P., & Gehrels, R. W. (2016). Two-dimensional seismic refraction tomography of a buried bedrock valley at Hallsands beach, Devon, United Kingdom. Environmental Geosciences, 23(4), 179-193.
14. Azwin, I., Saad, R., & Nordiana, M. (2013). Applying the seismic refraction tomography for site characterization. APCBEE procedia, 5, 227-231.
15. Borcherdt, R. D. (1994). Estimates of site-dependent response spectra for design (methodology and justification). Earthquake spectra, 10(4), 617-653.
16. Christensen, N. I., & Stanley, D. (2003). Seismic velocities and densities of rocks. In International Geophysics (Vol. 81, pp. 1587-1594): Elsevier.
17. Clayton, C. R., Simons, N. E., & Matthews, M. C. (1982). Site investigation: Granada.
18. Davis, J. L., & Annan, A. P. (1989). Ground-penetrating radar for high-resolution mapping of soil and rock stratigraphy 1. Geophysical prospecting, 37(5), 531-551.
19. Davis, R. (1995). Effects of weathering on site response. Earthquake engineering structural dynamics, 24(2), 301-309.
20. Junner, N. R., & Bates, D. A. (1941). The Accra earthquake of 22nd June, 1939: FJ Miller.
21. Kanlı, A. I., Tildy, P., Prónay, Z., Pınar, A., & Hermann, L. (2006). VS 30 mapping and soil classification for seismic site effect evaluation in Dinar region, SW Turkey. Geophysical Journal International, 165(1), 223-235.Kassie, L. N. (2019).
22. Kassie, L. N. (2019). Near-Surface Seismic Refraction Tomography; a case study for geotechnical application. Journal of Geotechnical Engineering, 6(2), 18-26.
23. Keary, P., Brooks, M., & Hill, I. (2002). An Introduction to Geophysical Exploration, Blackwell Science, 2002. ISBN0632049294.

24. Kutu, J. M. (2013). Seismic and tectonic correspondence of major earthquake regions in southern Ghana with Mid-Atlantic transform-fracture zones. International Journal of Geosciences, 2013
25. Leucci, G., Greco, F., De Giorgi, L., & Mauceri, R. (2007). Three-dimensional image of seismic refraction tomography and electrical resistivity tomography survey in the castle of Occhiola (Sicily, Italy). Journal of Archaeological Science, 34(2), 233-242.
26. Loke, M. (1999). Electrical imaging surveys for environmental and engineering studies. 2.
27. Loke, M., Chambers, J., Rucker, D., Kuras, O., & Wilkinson, P. (2013). Recent developments in the direct-current geoelectrical imaging method. Journal of applied geophysics, 95, 135-156.
28. Malehmir, A., Bastani, M., Krawczyk, C. M., Gurk, M., Ismail, N., Polom, U., & Perss, L. (2013). Geophysical assessment and geotechnical investigation of quick-clay landslides–a Swedish case study. Near Surface Geophysics, 11(3), 341-352.
29. Martin, A. J., & Diehl, J. G. (2004). Practical experience using a simplified procedure to measure average shear-wave velocity to a depth of 30 meters (VS30). Paper presented at the 13th World Conf. on Earthquake Engineering.
30. Martínez, K., & Mendoza, J. A. (2011). Urban seismic site investigations for a new metro in central Copenhagen: Near-surface imaging using reflection, refraction and VSP methods. Physics
31. McPherson, A., & Hall, L. (2013). Site classification for earthquake hazard and risk assessment in Australia. Bulletin of the Seismological Society of America, 103(2A), 1085-1102.
32. Milsom, J. (2003). Field geophysics (Vol. 31): John Wiley & Sons.
33. Muchingami, I., Hlatywayo, D., Nel, J., & Chuma, C. (2012). Electrical resistivity survey for groundwater investigations and shallow subsurface evaluation of the basaltic-greenstone formation of the urban Bulawayo aquifer. Physics and Chemistry of the Earth, Parts A/B/C, 50, 44-51.
34. Nazarian, S., Stokoe II, K. H., & Hudson, W. R. (1983). Use of spectral analysis of surface waves method for determination of moduli and thicknesses of pavement systems.

35. NEHRP. (2003). NEHRP Recommended Provisions For Seismic Regulations For New Buildings And Other Structures (Fema 450).
36. Nordiana, M., Bery, A., Taqiuddin, Z., Jinmin, M., & Abir, I. (2018). 2-D electrical resistivity tomography (ERT) assessment of ground failure in an urban area. Paper presented at the Journal of Physics: Conference Series.
37. Nortey, G., Armah, T. K., & Amponsah, P. (2018). Vs30 mapping at selected sites within the Greater Accra Metropolitan Area. Journal of African Earth Sciences, 142, 158-169
38. Nusret, D., & Dug, S. (2012). Applying the inverse distance weighting and kriging methods of the spatial interpolation on the mapping the annual precipitation in Bosnia and Herzegovina
39. Olafsdottir, E. A., Bessason, B., & Erlingsson, S. (2018). Combination of dispersion curves from MASW measurements. Soil Dynamics and Earthquake Engineering, 113, 473-487.Osae, S.,
40. Osae, S., Asiedu, D. K., Banoeng-Yakubo, B., Koeberl, C., & Dampare, S. B. (2006). Provenance and tectonic setting of Late Proterozoic Buem sandstones of southeastern Ghana: Evidence from geochemistry and detrital modes. Journal of African Earth Sciences, 44(1), 85-96.
41. Palmström, A. (1996). Application of seismic refraction stjrvey in assessment of jointing
42. Pomposiello, C., Dapeña, C., Favetto, A., & Boujon, P. (2012). Application of geophysical methods to waste disposal studies. Municipal and Industrial Waste Disposal, 3-26.
43. Quaah, A. O. (1982). A study of past major earthquakes in southern Ghana using intensity data. Tectonophysics, 88(1-2), 175-188.
44. Reynold, J. M. (2011). An introduction to applied and environmental geophysics: John Wiley & Sons
45. Rodri´ guez-Marek, A., Bray, J. D., & Abrahamson, N. A. (2001). An empirical geotechnical seismic site response procedure. Earthquake spectra, 17(1), 65-87
46. Shebl, S., Gemail, K., Attwa, M., Soliman, S. A., Azab, A., & Farag, M. (2019). Utilizing shallow seismic refraction in defining the geotechnical properties of the foundation

materials: A case study at New Minia City, Nile Valley, Egypt. Egyptian Journal of Petroleum, 28(2), 145-154.

47. Soupios, P., Georgakopoulos, P., Papadopoulos, N., Saltas, V., Andreadakis, A., Vallianatos, F., . . Engineering. (2007). Use of engineering geophysics to investigate a site for a building foundation. 4(1), 94-103.
48. Steidl, J. H., Tumarkin, A. G., & Archuleta, R. (1996). What is a reference site? Bulletin of the Seismological Society of America, 86(6), 1733-1748.
49. Taipodia, J., Dey, A., Gaj, S., Baglari, D. J. C., & Geosciences. (2020). Quantification of the resolution of dispersion image in active MASW survey and automated extraction of dispersion curve. 135, 104360.
50. Tyler, S., Vanneste, M. and Butler, D. (2017). Geophysical Techniques for Offshore Site Investigation. In Encyclopedia of Maritime and Offshore Engineering (eds J. Carlton, P. Jukes and Y.S. Choo). https://doi.org/10.1002/9781118476406.emoe525
51. Vickery, A. C., & Hobbs, B. A. (2002). The effect of subsurface pipes on apparent-resistivity measurements. Geophysical Prospecting, 50(1), 1-13.
52. Volti, T., Burbidge, D., Collins, C., Asten, M., Odum, J., Stephenson, W., . . . Holzschuh, J. (2016). Comparisons between VS 30 and spectral response for 30 sites in Newcastle, Australia, from collocated seismic cone penetrometer, active-and passive-source VS data. Bulletin of the Seismological Society of America, 106(4), 1690-1709
53. Zhang, J., & Toksöz, M. N. (1998). Nonlinear refraction traveltime tomography. Geophysics, 63(5), 1726-1737.